THE ASTROPHYSICAL JOURNAL, 567:999–1012, 2002 March 10
© 2002. The American Astronomical Society. All rights reserved. Printed in U.S.A.

DISCOVERY OF REFLECTION NEBULOSITY AROUND FIVE VEGA-LIKE STARS

PAUL KALAS AND JAMES R. GRAHAM
Astronomy Department, University of California, 601 Campbell Hall, Berkeley, CA 94720; and Center for Adaptive Optics, University of California, Santa Cruz, CA 95064

STEVEN V. W. BECKWITH
Space Telescope Science Institute, 3700 San Martin Drive, Baltimore, MD 21218

DAVID C. JEWITT
Institute for Astronomy, University of Hawaii, 2680 Woodlawn Drive, Honolulu, HI 96822

AND

JAMES P. LLOYD
Astronomy Department, University of California, 601 Campbell Hall, Berkeley, CA 94720; and Center for Adaptive Optics, University of California, Santa Cruz, CA 95064

Received 2000 October 11; accepted 2001 October 31

ABSTRACT

Coronagraphic optical observations of six Vega-like stars reveal reflection nebulosities, five of which were previously unknown. The nebulosities illuminated by HD 4881, HD 23362, HD 23680, HD 26676, and HD 49662 resemble that of the Pleiades, indicating an interstellar origin for dust grains. The reflection nebulosity around HD 123160 has a double-arm morphology, but no disklike feature is seen as close as 2.″5 from the star in *K*-band adaptive optics data. We demonstrate that a uniform density dust cloud surrounding HD 23362, HD 23680, and HD 123160 can account for the observed 12–100 μm spectral energy distributions. For HD 4881, HD 26676, and HD 49662, an additional emission source, such as from a circumstellar disk or nonequilibrium grain heating, is required to fit the 12–25 μm data. These results indicate that in some cases, particularly for Vega-like stars located beyond the Local Bubble (>100 pc), the dust responsible for excess thermal emission may originate from the interstellar medium rather than from a planetary debris system.

Subject headings: circumstellar matter — infrared: ISM — infrared: stars — instrumentation: adaptive optics — reflection nebulae

1. INTRODUCTION

The far-infrared (FIR), all-sky survey conducted by the *Infrared Astronomical Satellite* (*IRAS*) revealed that roughly 15% of nearby main-sequence stars have excess thermal emission due to the presence of circumstellar dust (Backman & Gillett 1987; Aumann 1988; Plets 1999). The thermal excess was first discovered around Vega (Aumann et al. 1984), and approximately 100 main-sequence stars display the "Vega phenomenon" (Backman & Paresce 1993). The spectral energy distributions (SEDs) of Vega-like stars are typically fitted assuming disklike distributions of grains (Sylvester & Skinner 1996), although in the optically thin regime the adopted geometry plays no role. Assuming the grains orbit the host stars as circumstellar disks, the dust destruction timescales are typically 1 or 2 orders of magnitude shorter than the stellar ages. The existence of unseen parent bodies, exosolar analogs to Kuiper belt objects, is inferred in order to replenish the dust complex via collisional erosion (Backman & Paresce 1993).

High-resolution imaging of Vega-like stars has confirmed the existence of circumstellar debris disks around roughly seven main-sequence stars (Kalas 1998; Lagrange, Backman, & Artymowicz 2000). However, the ratio of debris disks inferred from the FIR SEDs to those spatially resolved by imaging is approximately 10:1. Here we present coronagraphic images of reflection nebulosity surrounding six main-sequence stars previously identified as Vega-like (Backman & Paresce 1993; Sylvester et al. 1996). The new data show dust morphology that is not disklike but qualitatively resembles the Pleiades reflection nebulosity in five cases. Dust-scattered light detected around HD 123160 shares characteristics with nebulosities seen in both the Pleiades and star-forming regions.

2. OBSERVATIONS AND DATA REDUCTION

We used an optical coronagraph at the University of Hawaii (UH) 2.2 m telescope to obtain CCD images in the *R* band (Table 1). HD 123160 was also imaged in the *V* band. Reimaging optics gave 0.″4 pixel^{-1}, sufficient to Nyquist sample the ~1.″2 full width at half-maximum (FWHM) point-spread function (PSF). The field of view was a circular region with a diameter of 5.′5.

Follow-up observations were obtained in the near-infrared (NIR) for HD 123160 using the Lick Observatory 3 m telescope (Table 1). A 256 × 256 pixel (0.″076 pixel^{-1}), coronagraphic, NIR camera was used to artificially eclipse the central star with a 0.″7 wide finger (Lloyd et al. 2000). Adaptive optics compensation (Max et al. 1997) using the primary star as a wave front reference source improved image quality from ~1″ intrinsic seeing to ~0.″16 (FWHM).

Our target sample was compiled from lists of Vega-like stars published by Sylvester et al. (1996) and Backman & Paresce (1993). We imaged all 22 Vega-like stars from Table 16 in Sylvester et al. (1996) and 38 of the 60 stars from Table VIII in Backman & Paresce (1993). The total sample of 79 stars (the two tables have three stars in common) includes several with resolved debris disks (β Pic, Vega, ϵ Eri, and Fomalhaut), two members of the Pleiades (18 Tau and 21 Tau), and three Herbig Ae/Be stars (HD 34282, HD

TABLE 1

SUMMARY OF OBSERVATIONS

Name	Date (UT)	Telescope	λ (μm)	R_{in}[a] (arcsec)	Integration (s)	Spectral Type	Parallax (mas)	Nebulosity
HD 4881	1993 Oct 12	UH 2.2 m	0.65	4.0	640	B9.5 V	2.84	Pleiades
HD 23362	2000 Jan 30		0.65	4.5	285	K2 V	3.24	Pleiades
HD 23680	2000 Jan 30		0.65	4.5	600	G5 V	5.54	Pleiades
HD 26676	1993 Oct 12		0.65	4.0	320	B8 Vn	6.49	Pleiades
HD 49662	2000 Jan 30		0.65	6.7	640	B7 IV	5.37	Pleiades
HD 123160.....	2000 Jan 29		0.65	4.1	510	G5 V	-0.01[b]	Double arm
	2000 Jan 30		0.55	3.7	120			
	2000 Jun 17	Lick 3.0 m	2.15	2.5	360			
	2001 Jun 3		2.15	4.0	720			
	2001 Jun 3		1.66	4.0	600			

[a] Radius from target star blocked by coronagraphic occulting spot and PSF residuals.
[b] Negative value in *Hipparcos Catalog* indicates parallax measurement that is smaller than the error. In § 4.6 we estimate $d \sim 110$ pc.

35187, and HD 141569). We also observed stars nearby in the sky and with magnitudes comparable to the science targets to be used later as template stars for PSF subtraction.

Data reduction followed the standard steps of bias subtraction, flat-fielding, sky subtraction, image registration, and median-filtering of multiple frames to attain the effective integration times listed in Table 1. The PSF of each science target was subtracted either by using template PSFs discussed above or by radially sampling the template PSF, fitting the data with a seventh-order polynomial, and producing an artificial PSF from this fit. The PSF subtraction step is useful for extracting faint nebulosity as close to the star as possible, but the nebulosities discussed here are detected in raw data. Residual noise after the PSF subtraction dominates the data $\sim 1''$ beyond the edge of the occulting spot. Table 1 lists the radius centered on each target star below which we cannot obtain reliable information about the circumstellar environment.

3. RESULTS

The suppression of direct stellar light with the coronagraph reveals the presence of faint reflection nebulosity around the six Vega-like stars in Table 1 and Figure 1. The nebulosites have the following general properties: (*a*) spatial extent $\sim 1'$–$2'$ radius; (*b*) surface brightness varying as radius, $r^{-\beta}$, with $\beta \leq 2$; (*c*) range of surface brightness approximately 20–24 mag arcsec^{-2}; and (*d*) linear, filamentary, striated morphological structure, similar to that observed in the Pleiades reflection nebulosities (Arny 1977). The background noise, 3 $\sigma \sim 24$ mag arcsec^{-2}, limits the radial extent to which each nebulosity is detected. Table 1 gives the *Hipparcos* parallaxes, indicating heliocentric distances greater than 100 pc for every star. The detected nebulosities therefore span spatial scales of 10^3–10^5 AU from their parent stars, and the occulted regions obscure the central $\sim 10^3$ AU (Table 1).

The nebulosity around HD 26676 (Fig. 1D), the brightest and most extended, has been previously documented by van den Bergh (1966) and identified as a member of the Tau R2 association (Racine 1968), which is part of the Pleiades. An examination of the literature indicates that the other five nebulosities were not previously known.

The nebulosity around HD 123160 is characterized by a double-arm structure southeast of the star (Fig. 1F; features i and ii), rather than the linear features seen around the other five stars. Armlike morphologies appear near several pre–main-sequence stars such as GM Aur and Z CMa (Nakajima & Golimowski 1995). The outside boundary of arm i traces a closed curve that intersects feature iii. The latter is curved in the same direction as feature i, indicating that iii may be a detached segment of feature i. Another diffuse, curved structure, iv, is 95″ from the star with position angle and curved morphology comparable to feature iii. Neither iii nor iv have a core + halo structure that characterizes background field galaxies in these data. We also detect two point sources lying along a north-south axis and separated by 3.″6 at position v. They are surrounded by a nebulosity that has a tail pointing toward HD 123160. Both are red, with $V-K = 1.7$ mag and 1.1 mag for the north and south stars, respectively (after applying the extinction correction determined for HD 123160 in Table 3). The colors of the northern component are consistent with a late-type stellar photosphere. However, the southern component has $H-K = 1.1$ mag, indicating an additional source of NIR emission such as from a circumstellar disk (Meyer, Calvet, & Hillenbrand 1997).

Figure 2 shows that two brightness knots exist within arm ii. In the *K*-band adaptive optics data, the north knot, iia, contains a pointlike source $9.''7 \pm 0.''2$ from the star superposed on the broader nebular emission. After subtracting an estimate for the background contributed by the broader nebulosity, the pointlike source has $V = 16.5 \pm 0.3$ mag and $K = 14.2 \pm 0.3$ mag (extinction corrected; Table 3). The $V-K$ color is consistent with a K dwarf spectral type and distance modulus of greater than 100 pc. Compared to the optical data, the adaptive optics *K*-band data probe closer to the star for any structure that may have a disklike morphology. No circumstellar disk is detected as close as $\sim 2.''5$ from the primary.

Aperture photometry (diameter = 4.″0) performed on the nebulosities labeled in Figures 1F and 2 gives *R*- and *V*-band fluxes that decrease radially from the star with $\beta \leq 1$, rather than $\beta = 2$ or $\beta = 3$, which would characterize a homogenous medium or dust disk, respectively. For example, feature iii has 9% of the flux of feature iia, but is 5 times farther from the primary. If both features are produced by grains with similar scattering properties, then iii has approximately twice as many scattering grains as iia. The $V-R$ colors range from 0.0 to -0.2 mag after an extinction correction is applied. Using $R = 7.81$ mag for HD 123160 (Sylvester et al. 1996), $V-R = +0.2$ mag if HD

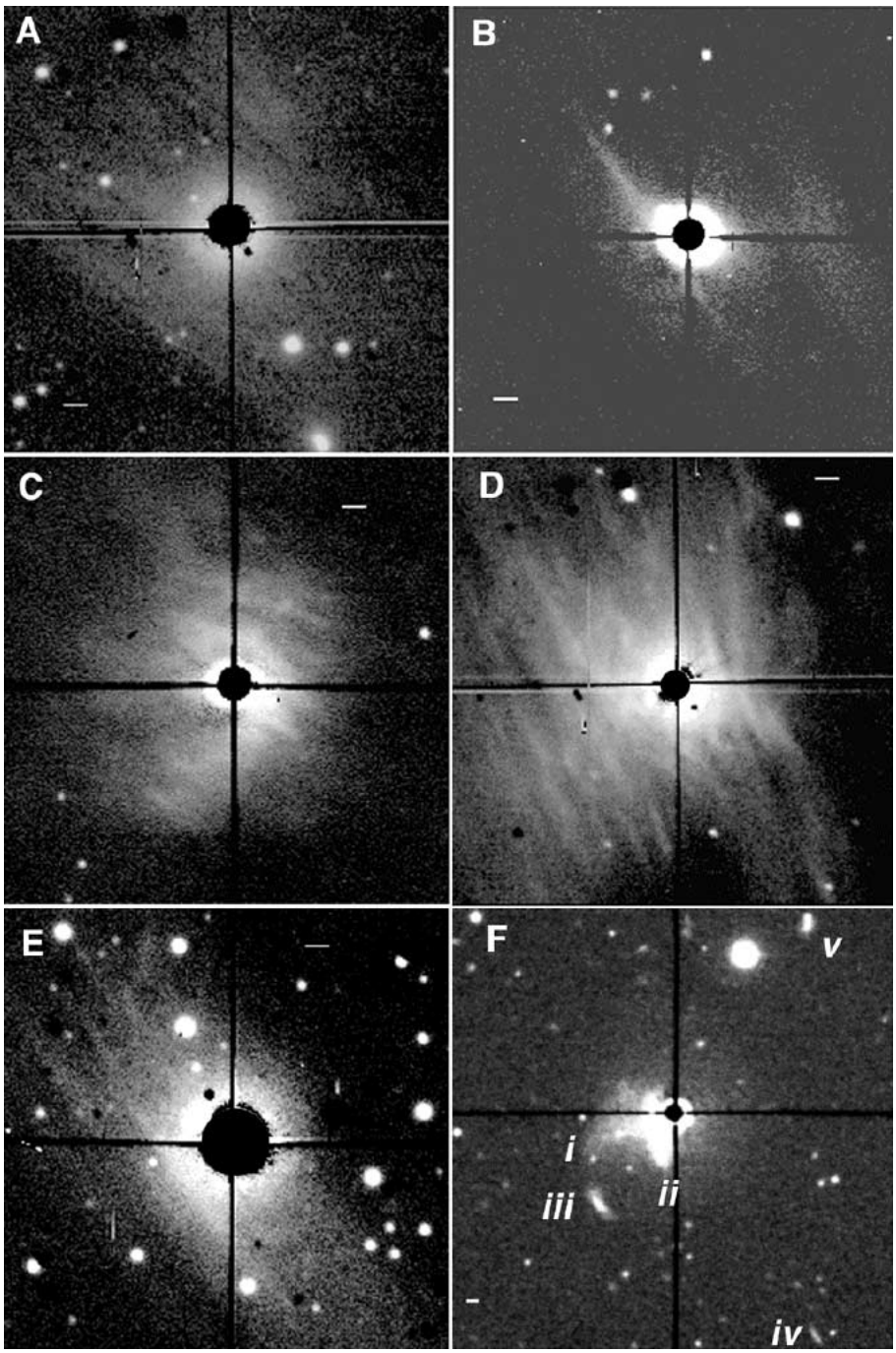

FIG. 1.—*R*-band coronagraphic images of six Vega-like stars after PSF subtraction (A: HD 4881, B: HD 23362, C: HD 23680, D: HD 26676, E: HD 49662, F: HD 123160). North is up, east is left, the white bar represents 5″, and each box is 1.′5 on a side, except for F, which is 3.′0 on a side. For F we label five regions of nebulosity discussed in the text. Negative features are artifacts of the PSF subtraction step.

123160 is a G5 V star, or $V-R=+0.3$ mag if it is a G0 III star. Therefore, the nebulous features in Figures 1F and 2 appear bluer than HD 123160, consistent with the scattered-light colors of the Merope Nebula (Herbig 1996; Herbig & Simon 2001).

The discovery of nebulosity around these Vega-like stars that is not disklike raises the question of whether or not the dust emitting in the FIR is contained in disks related to planet building, or merely due to dust contained in the interstellar medium (ISM). The "Pleiades phenomenon" is due to the chance encounter of bright, nearby stars with a clump of ISM (Arny 1977; White & Bally 1993; Herbig & Simon 2001). Filamentary features in optical scattered light are produced by the shearing of the cloud as radiation pressure pushes dust around each star. Our data do not necessarily exclude the existence of circumstellar disks in addition to the Pleiades-like nebulosity because the observations are not sensitive to the central $\sim 4''$ radius (Table 1). However, the main reason to presume the existence of a circumstellar disk is that the *IRAS* data give fluxes in excess

TABLE 2

OPTICAL THROUGH FAR-INFRARED FLUXES (NOT DEREDDENED OR COLOR CORRECTED)

	FLUX (mag)								FLUX (Jy)			
NAME	0.44 μm	0.55 μm	0.88 μm	1.22 μm	1.65 μm	2.18 μm	3.55 μm	4.77 μm	12 μm	25 μm	60 μm	100 μm
HD 4881	...	...	...	...	...	...	...	...	0.28	0.28	3.88	11.2
	6.25	6.22	6.17	5.99	5.99	5.96	...	...	0.36	0.39	4.75	11.5
HD 23362	9.53	7.85	6.07	...	...	...	3.72	3.98	1.42	0.50	0.67	2.88
	9.62	7.91	6.18	4.89	4.05	3.85	...	...	1.38	0.44	0.72	6.32
HD 23680	9.40	8.60	...	6.01	5.37	5.24	5.16	5.29	0.44	...	1.89	6.27
	9.62	8.39	7.20	...	...	...	...	...	0.43	0.19	2.08	6.02
HD 26676	...	...	...	...	...	...	...	...	1.15	6.43	26.3	37.2
	6.26	6.24	6.20	...	...	...	...	...	1.49	7.41	30.0	47.4
HD 49662	5.30	5.40	...	5.7	5.5	5.6	5.8	...	0.43	1.62	4.60	5.68
	5.29	5.39	5.47	...	5.61	5.59	...	...	...	...	...	...
HD 123160.....	10.12	8.62	6.94	5.86	5.07	4.87	4.73	5.33	0.60	0.38	3.03	3.97
	10.25	8.66	7.05	...	...	...	...	...	0.62	0.37	3.11	4.41
18 Tau	...	...	...	...	...	...	...	...	0.47	0.59	2.99	6.01
	5.60	5.66	5.69	...	...	...	...	...	0.42	0.74	3.52	12.80
21 Tau	...	...	...	...	...	...	...	...	0.42	1.14	4.68	10.90
	5.72	5.76	5.74	...	...	...	...	...	0.39	1.06	13.20	9.75

NOTE.—0.44–0.88 μm from Sylvester et al. (1996) (first row) and *Hipparcos* (second row); 1.22–2.18 μm from Sylvester et al. (1996) (first row) and 2MASS (second row); 3.55–4.77 μm from Sylvester et al. (1996); 12–100 μm fluxes from *IRAS* PSC (first row) and *IRAS* FSC (second row).

of photospheric levels. If the Pleiades-like dust detected here is capable of producing the FIR emission, then the Pleiades phenomenon is a more plausible explanation for the FIR excesses than the Vega phenomenon. Below we test the validity of attributing the observed excess FIR emission to an interstellar dust cloud encountering each of our target stars.

4. THERMAL EMISSION MODEL FOR THE PLEIADES PHENOMENON

To test if the *IRAS* FIR data are consistent with the Pleiades phenomenon, we experiment with a model comprising a star embedded in a uniform number density, optically thin, dust cloud. The geometry is spherical, except that

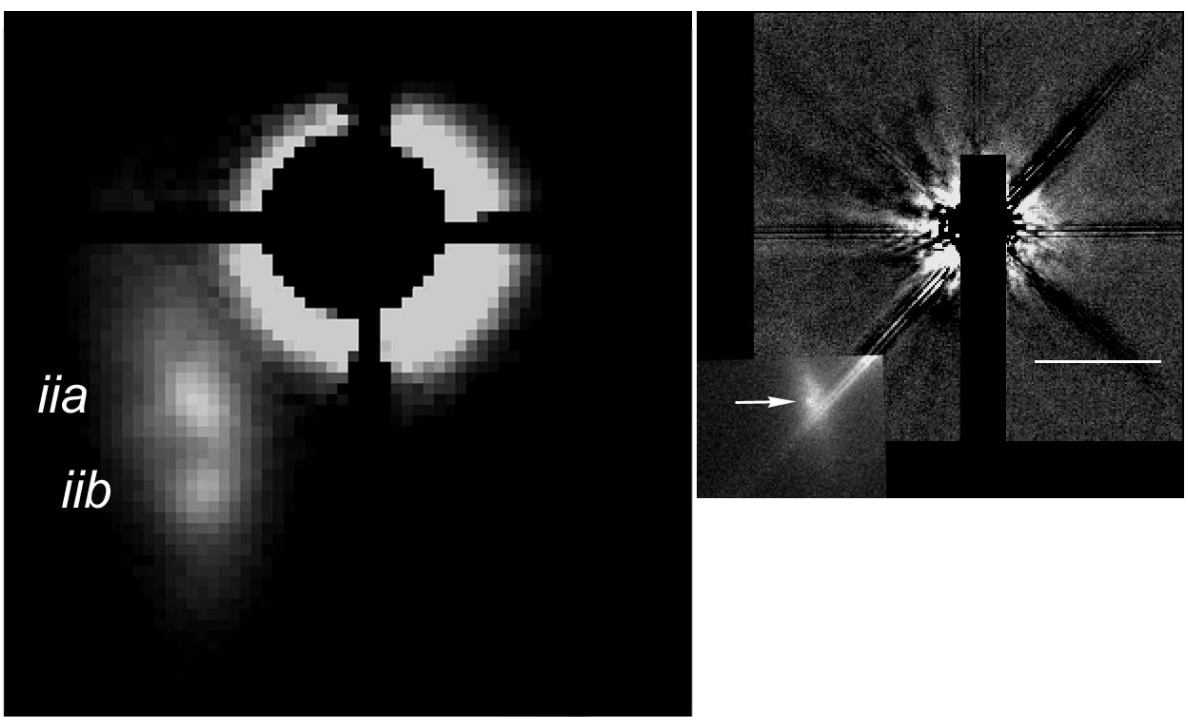

FIG. 2.—The left panel is a different gray-scale stretch and field of view of Fig. 1F, showing the existence of two brightness peaks within arm ii. The right panel shows the same field imaged with adaptive optics at 2.15 μm on two different nights. The wide field shows the 2000 June 17 data, where HD 123160 was placed behind the occulting finger and a PSF template was subtracted to search for disklike nebulosity. In the lower left of this frame we superpose the 2001 June 3 *K*-band data, which has higher signal-to-noise ratio due to the greater integration time (Table 1) and the fact that no PSF template is subtracted. In both *K*-band data sets, as well as the *H*-band data, feature iia is detected as a possible point source at P.A. ~ 135°, indicated here with an arrow. The white bar represents 5″.

radiation pressure from the star excavates an axisymmetric paraboloidal cavity within the cloud, as described by Artymowicz & Clampin (1997). In spherical coordinates, (r, θ, ϕ), a volume element is given as $dV = dr \times r\,d\theta \times r \sin\theta\,d\phi$. The inner boundary of the cloud cavity has radius

$$r = r_{\rm in}\left(\frac{2}{1+\cos\theta}\right). \quad (1)$$

The smallest radius that grains can approach the star, $r_{\rm in}$, depends on the relative velocity and the force of radiation pressure (which scales with stellar luminosity and grain properties, such as size). For example, at a relative velocity of 12.2 km s^{-1}, grains less than 0.2 μm in size will not approach Vega closer than $\sim$2000 AU, whereas 1 μm sized grains will reach as close as $\sim$200 AU (Artymowicz & Clampin 1997). In our simulations $r_{\rm in}$ is a free parameter.

Grain temperatures are calculated in each volume element assuming grains receive blackbody radiation from the star and emit as blackbodies. Grain absorption and emission efficiences will depend on grain properties and wavelength regimes. We estimate the absorption and emission efficiencies empirically by assuming that they have the same functional form as the extinction function for interstellar grains given by Mathis (1990) in his Table 1. A smoothed version of this extinction function can be described by three power laws with form $\epsilon(\nu) = \epsilon_0\,\nu^{\alpha}$, where $\alpha = 0$ for $\lambda < 0.5$ μm, $\alpha = 1.68$ for $0.5\mu{\rm m} \le \lambda < 5\mu{\rm m}$, and $\alpha = 1.06$ for $\lambda \ge 5\mu{\rm m}$. Very hot stars will put out their energy at short wavelengths where the grain absorption efficiency is at a maximum, whereas cool stars will not efficiently heat these interstellar grains. Most of the energy re-radiated by grains will occur in the $\lambda \ge 5$ μm regime, and therefore will have emission efficiency proportional to $\nu^{1.06}$.

The dust cloud thermal emission is fitted to the observed *IRAS* fluxes by adjusting the grain number density, ρ, the inner minimum radius of the cavity, $r_{\rm in}$, and the outer radius of the cloud, $R_{\rm out}$. The photospheric contribution from optical wavelengths through 12 μm is fitted by adjusting the stellar temperature, radius, and heliocentric distance. In the first iteration, the stellar temperature and radius are taken from Cox (1999) based on the spectral type for each star given in the literature.

Table 2 gives the observed optical, NIR, and FIR magnitudes and fluxes. Interstellar reddening and extinction were calculated using both the $B-V$ and $V-K$ colors and is given in Table 3; we used $R_V = 3.1$ for the total-to-selective extinction values given by Mathis (1990) in his Table 1. The color correction for the FIR data was obtained from Table VI.C.6 in the *IRAS Explanatory Supplement Version 2*. In Table 4 we list the extinction-corrected optical and NIR photometry and the *IRAS* fluxes color-corrected based on the temperatures listed in Table 1. In several cases an alternative spectral type is proposed, and the extinction and photometry are recalculated. We considered both the *IRAS* Point Source Catalogue (PSC) and the Faint Source Catalogue (FSC) data for fitting the model to the 12–100 μm fluxes. The uncertainties for these data are given in the respective *IRAS* catalogs, with typical values of $\sim$10%. The heliocentric distances used in the first iteration are taken from the *Hipparcos* parallaxes for each star (Table 1), but beyond 100 pc the *Hipparcos* distances have significant uncertainties.

Table 5 gives two examples of model fits to the SED of each star, and Figures 3–10 display the model fits as discussed below. Table 5 also lists the maximum grain temperature, T_0, the fractional infrared luminosity of the cloud, L_d/L_*, and the maximum optical depth, $\tau_{\rm max}$. For HD 4881, HD 26676, and HD 49662, the model fits to the 60–100 μm emission give a deficit of 12–25 μm emission. Our simple model assumptions do not account for at least four factors that could enhance the 12–25 μm emission.

First, density variations exist within the dust cloud, as shown in the optical images (Fig. 1). The theoretical model of Artymowicz & Clampin (1997) also shows that a "snowplow" effect occurs as the dust moves around the cavity maintained by radiation pressure. A skin of higher density material will exist near the surface of the cavity. If we assume that the cavity is a sphere for simplicity, and displace the material that would have occupied the sphere to an annular skin with thickness $\Delta r = r_s - r_{\rm in}$, then the mass density in the skin is

$$\frac{\rho_{\rm skin}}{\rho_{\rm cloud}} = 1 + \left(\frac{r_{\rm in}^3}{r_s^3 - r_{\rm in}^3}\right). \quad (2)$$

TABLE 3

EXTINCTION ASSUMING $A_V = 3.0E(B-V)$ AND $A_V = 1.1\,(V-K)$

NAME	SPECTRAL TYPE	$B-V$ Observed	$(B-V)_0$	$E(B-V)$	$V-K$ Observed	$(V-K)_0$	$E(V-K)$	A_V	
								$B-V$	$V-K$
HD 4881	B9.5 V	0.03	−0.07	0.10	0.26	−0.13	0.39	0.30	0.43
	B8 V		−0.11	0.14		−0.24	0.50	0.42	0.55
HD 23362	K2 V	1.70	0.91	0.79	4.03	2.22	1.81	2.37	1.99
	K2 III		1.16	0.54		2.70	1.33	1.62	1.46
HD 23680	G5 V	1.01	0.68	0.33	3.26	1.59	1.67	0.99	1.84
	G5 III		0.86	0.15		2.10	1.16	0.45	1.28
HD 26676	B8 Vn	0.02	−0.11	0.13	...	...	...	0.39	...
HD 49662	B7 IV	−0.10	−0.14	0.04	−0.20	−0.29	0.09	0.12	0.10
HD 123160.....	G5 V	1.55	0.68	0.87	3.77	1.59	2.18	2.61	2.40
	G0 III		...	...		1.75	2.02	...	2.22
18 Tau	B8 V	−0.06	−0.11	0.05	...	...	...	0.15	...
21 Tau	B8 V	−0.04	−0.11	0.07	...	...	...	0.21	...

NOTE.—The observed magnitudes used here are the average of the two values given for each passband in Table 2. A_V from $V-K$ was used to determine A_λ for Table 4 except when $V-K$ data are not available.

TABLE 4

DEREDDENED OPTICAL AND NIR MAGNITUDES AND COLOR-CORRECTED FIR FLUXES

NAME	SPECTRAL TYPE	FLUX (mag)								FLUX (Jy)			
		0.44 μm	0.55 μm	0.88 μm	1.22 μm	1.65 μm	2.18 μm	3.55 μm	4.77 μm	12 μm	25 μm	60 μm	100 μm
HD 4881	B9.5 V	...	...	...	...	...	...	...	...	0.19	0.20	2.94	10.28
		5.69	5.79	5.97	5.87	5.92	5.91	...	...	0.25	0.27	3.60	10.55
	B8 V	...	...	...	...	...	...	...	...	...	...	...	...
		5.54	5.67	5.91	5.84	5.90	5.90	...	...	...	...	...	...
HD 23362	K2 V	6.90	5.86	5.12	...	...	...	3.63	3.93	1.00	0.36	0.51	2.64
		6.99	6.45	5.23	4.33	3.70	3.64	...	...	0.97	0.31	0.54	5.80
	K2 III	7.60	6.39	5.37	...	...	...	3.65	3.94	...	...	...	...
		7.69	6.45	5.48	4.48	3.79	3.69	...	...	...	...	...	...
HD 23680	G5 V	6.96	6.76	...	5.49	5.05	5.04	5.07	5.24	0.31	...	1.43	5.75
		7.18	6.55	6.32	...	...	...	...	...	0.30	0.13	1.58	5.52
	G0 III	7.71	7.32	...	5.65	5.15	5.10	5.10	5.26	...	...	...	...
		7.93	7.11	6.59	...	...	...	...	...	...	...	...	...
HD 26676	B8 Vn	...	...	...	...	...	...	...	...	0.79	4.56	19.92	34.13
		5.74	5.85	6.01	...	...	...	...	...	1.03	5.26	22.73	43.49
HD 49662	B7 1V	5.16	5.30	...	5.67	5.48	5.59	5.79	...	0.30	1.15	3.48	5.21
		5.15	5.29	5.42	...	5.59	5.58	...	...	...	...	...	...
HD 123160...	G5 V	6.92	6.22	5.78	5.18	4.68	4.61	4.61	5.27	0.42	0.27	2.30	3.64
		7.05	6.26	5.89	...	...	...	...	...	0.43	0.26	2.36	4.04
	G0 III	7.16	6.40	5.87	5.23	4.68	4.63	4.62	5.27	...	...	...	...
		7.29	6.44	5.98	...	...	...	...	...	...	...	...	...
18 Tau	B8 V	...	...	...	...	...	...	...	...	0.33	0.42	2.27	5.51
		5.40	5.51	5.62	...	...	...	...	...	0.29	0.53	2.67	11.74
21 Tau	B8 V	...	...	...	...	...	...	...	...	0.29	0.81	3.55	10.00
		5.62	5.55	5.64	...	...	...	...	...	0.27	0.75	10.00	8.94

NOTE.—Table rows have same format as Table 2, except that a second spectral type is given for several stars. The change in the FIR color correction for the second spectral type is negligible and not listed.

The larger the dust cavity produced by the star, the denser the skin layer for a fixed skin thickness. For example, ρ is a factor of 2 greater in the skin compared to the ambient cloud for $r_{in} = 200$ AU and $r_s = 250$ AU and a factor of 3 greater if we assume $r_{in} = 500$ AU and $r_s = 550$ AU. We find that including a high-density surface layer in the model increases the 12–25 μm emission slightly, but a good fit to the data requires a factor of $\sim 10^2$ increase in dust density between the skin and the ambient material. Thus, the enhanced 12–25 μm emission must have additional sources.

Second, larger grains (≥ 1 μm) will not be pushed back by radiation pressure and will occupy the cavity (Artymowicz & Clampin 1997). We find that filling the cavity with grains also does not succeed in fitting the observed 12–25 μm emission, given no increase in the density of material above the ambient medium (Table 5).

Third, the smallest grains (≤ 0.1 μm) will undergo nonthermal heating events to ~ 1000 K (Greenberg 1968; Sellgren 1984). The empirical finding for the Pleiades is that the 12–25 μm emission should represent $\sim 30\%$ of the total

TABLE 5

PLEIADES MODEL: UNIFORM DENSITY DUST CLOUD

Star-Model	T_{eff} (K)	d (pc)	R_* ($\times 10^{11}$ cm)	ρ ($\times 10^{-23}$) (g cm^{-3})	r_{in} (AU)	R_{out} (AU)	T_0 (K)	τ_{max}	L_d/L_*
HD 4881-a	12,300	168	2.09	0.27	800	1.0×10^5	146	1.6×10^{-3}	1.9×10^{-3}
HD 4881-b				0.29	300	8.7×10^4	217	1.5×10^{-3}	1.8×10^{-3}
HD 23362-a	4200	187	13.92	0.37	400	2.0×10^5	148	4.5×10^{-3}	2.0×10^{-3}
HD 23362-b				0.38	40	1.1×10^4	366	2.6×10^{-3}	1.2×10^{-3}
HD 23680-a	5050	205	6.97	2.30	200	7.0×10^4	176	9.8×10^{-3}	4.7×10^{-3}
HD 23680-b				3.20	400	4.0×10^4	134	7.7×10^{-3}	4.3×10^{-3}
HD 26676-a	11,600	163	2.09	2.50	100	5.5×10^4	320	8.4×10^{-3}	1.0×10^{-2}
HD 26676-b				22.0	50	3.0×10^3	421	4.0×10^{-3}	4.4×10^{-2}
HD 49662-a	14,000	180	2.47	0.13	100	6.2×10^4	397	4.9×10^{-4}	5.9×10^{-4}
HD 49662-b				0.70	10	1.1×10^4	1000	4.8×10^{-4}	5.7×10^{-4}
HD 123160-a	5,500	110	4.18	4.9	300	1.2×10^4	135	3.5×10^{-3}	2.1×10^{-3}
HD 123160-b.....		120		4.9	200	1.1×10^4	158	3.2×10^{-3}	2.0×10^{-3}
18 Tau-a	11,400	125	2.00	0.21	200	6.0×10^4	236	7.7×10^{-4}	2.2×10^{-5}
18 Tau-b				0.18	200	1.6×10^5	236	1.8×10^{-3}	1.9×10^{-5}
21 Tau-a	11,400	125	2.00	0.32	10	6.0×10^4	770	1.2×10^{-3}	4.3×10^{-5}
21 Tau-b				1.0	10	2.8×10^4	770	1.7×10^{-3}	1.3×10^{-4}

nebular FIR flux (Castelaz, Sellgren, & Werner 1987; Sellgren, Luan, & Werner 1990). The *IRAS* SEDs for four stars in the Pleiades show that the 12–25 μm flux densities lie significantly above a blackbody fitting the 60–100 μm data (Castelaz et al. 1987). Thus, a hot grain component could be present that will add 12–25 μm flux that is not accounted for by our model. However, the existence of small-grain heating should also produce observable NIR excess emission and infrared emission features (Desert et al. 1990; Sellgren, Werner, & Allamandola 1996; Sylvester, Skinner, & Barlow 1997).

Fourth, our simulation does not take into account the existence of a circumstellar disk in addition to the ISM nebulosity detected in this paper. Material close to the star with number density decreasing with radius would add 12–25 μm flux to our model SED. Future high-resolution observations are required to detect number density variations closer to the star than our observations permit (Table 1). In four cases below we discuss previous attempts to fit the SEDs with model circumstellar disks.

4.1. *18 Tau and 21 Tau*

Before applying our model to the stars shown in Figure 1, we test it on two Pleiads that are in the *IRAS* PSC and FSC and have been identified as candidate Vega-like stars (Backman & Paresce 1993). 18 Tau (HD 23324) and 21 Tau (HD 23432) are both B8 V stars with *Hipparcos* distances between 110 and 120 pc. Two model fits to the SED of each star are given in Figures 3 and 4 and Table 5. The parameters for models 18 Tau-a are chosen to produce a SED that fits the PSC 100 μm data. Model 18 Tau-b demonstrates that a fit to the FSC 100 μm point requires decreasing the mass density, ρ, and increasing the outer radius, $R_{\rm out}$, relative to model 18 Tau-a. However, no combination of parameters can fit the 12–25 μm and the 60–100 μm regions simultaneously, in agreement with the findings of Castelaz et al. (1987). These authors suggest that the nonequilibrium heating of small grains may account for the observed excess flux in the *IRAS* 12 and 25 μm passbands. The angular radii of models 18 Tau-a and 18 Tau-b would be 8′ and 21′, respectively. Gaustad & Van Buren (1993) measure 8′ radius for 18 Tau in the *IRAS* Infrared Sky Survey Atlas (ISSA). Thus, model 18 Tau-a is preferred over 18 Tau-b.

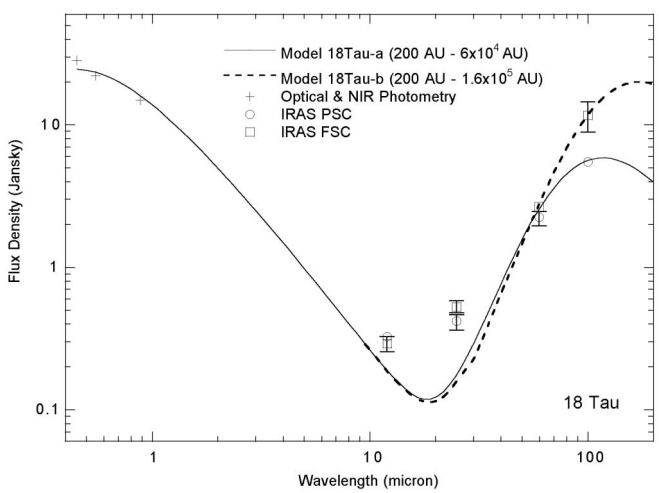

FIG. 3.—Photometric data for 18 Tau (Table 4) and spectral energy distributions from dust cloud models (Table 5). Symbol sizes for the *IRAS* data approximate the sizes of error bars unless marked otherwise. The two models demonstrate different cloud properties that give fits to either the PSC or FSC 100 μm data. However, the model cannot fit the 12–25 μm and 60–100 μm regions simultaneously, confirming previous findings (Castelaz et al. 1987). Nonequilibrium heating of small grains is thought to produce flux in excess of the 12–25 μm blackbody emission simulated here.

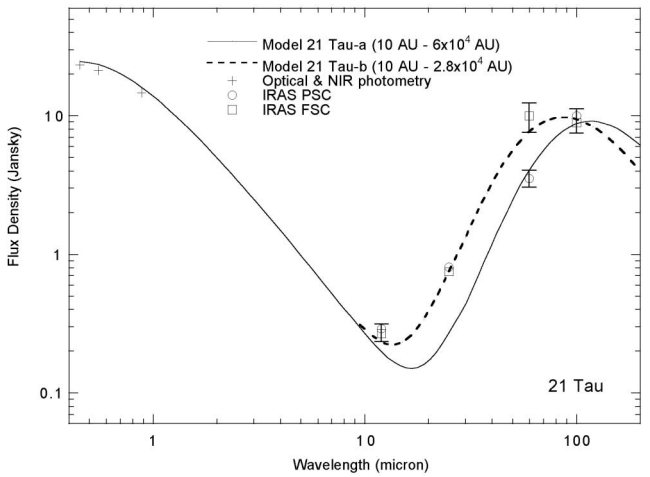

FIG. 4.—Photometric data for 21 Tau (Table 4) and spectral energy distributions from dust cloud models (Table 5). Symbol sizes for the *IRAS* data approximate the sizes of error bars unless marked otherwise. The two models demonstrate different cloud properties that give fits to either the PSC or FSC 100 μm data. For the *IRAS* PSC data, the observed SED is similar to that of 18 Tau (Fig. 3). Model 21 Tau-a has $r_{\rm in} = 10$ AU, but the hotter dust relative to the 18 Tau models (Fig. 3) does not produce enough 12–25 μm flux to fit the observations. A key difference in the *IRAS* FSC data for 21 Tau is the greater 60 μm flux density. This permits a fit to the entire SED with model 21 Tau-b (Table 5).

For a straightforward comparison, the model fits to the 21 Tau data use the same stellar parameters as the 18 Tau models. Model 21 Tau-a fits the *IRAS* 60–100 μm PSC data and again demonstrates that a second source of 12–25 μm emission is necessary. Relative to the 18 Tau models, we decrease the inner radius to 10 AU to show that the hotter grains do not add enough 12–25 μm flux to match the observations. However, the 60 μm flux density for 21 Tau in the *IRAS* FSC is significantly higher than in the PSC. Model 21 Tau-b gives a fit to the FSC data that agrees with the entire observed 12–100 μm SED. Thus the errors in any single FIR data point may change the physical interpretation significantly. The angular radii of models 21 Tau-a and 21 Tau-b would be 8′ and 3.′7, respectively. Gaustad & Van Buren (1993) measure 5′ radius for 21 Tau in ISSA maps. Thus, model 21 Tau-b is preferred over 18 Tau-a.

4.2. *HD 4881*

Given the B9.5 V spectral type for HD 4881, our model gives optical-NIR flux densities that lie well below the observed values if we assume the *Hipparcos* distance of 350 pc (Table 1) and $T_{\rm eff} = 11{,}400$ K. Rather, the fit to the optical and NIR data shown in Figure 5 assumes $d = 168$ pc and $T_{\rm eff} = 12{,}300$ K. The higher temperature is consistent with the Miroshnichenko et al. (1999) reclassification of this star as B8. The 25–100 μm fluxes are fitted with the dust cloud parameters given in Table 5. Figure 5 maps the spectral energy distributions of two model fits. Fitting the 100 μm photometry requires that R_{out} is not smaller than $\sim 8.7 \times 10^4$ AU. At the assumed distance, the model dust cloud subtends $\sim 8.'6$ radius, which is approximately equal to the average angular extent measured by Dring et al.

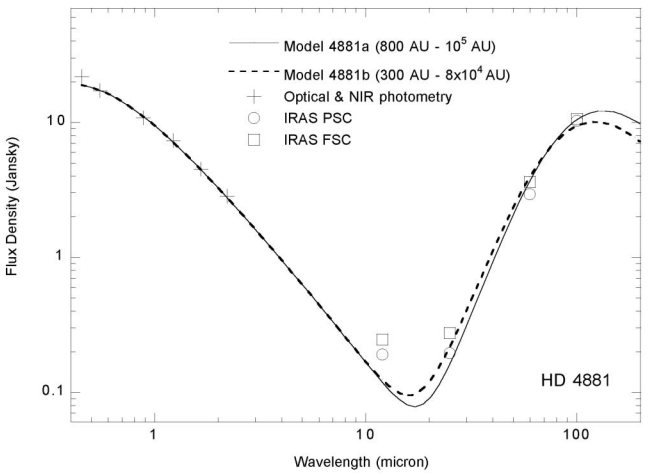

FIG. 5.—Photometric data for HD 4881 (Table 4) and spectral energy distributions from two dust cloud models (Table 5). Symbol sizes for the *IRAS* data approximate the sizes of error bars. The two models demonstrate different cloud dimensions that give SEDs consistent with the 25–100 μm data. Model 4881-b demonstrates that decreasing outer radius relative to model 4881a diminishes the 100 μm emission. Decreasing the inner radius in model 4881-b enhances the 25 μm emission, but with negligible effect on the 12 μm emission. The 12 μm emission should be mostly photospheric, but the *IRAS* data do not lie on the extrapolated photospheric blackbody curve.

(1996) in *IRAS* Skyflux plates. This is larger than the $\sim 5'$ radial extent measured by Gaustad & Van Buren (1993) and Miroshnichenko et al. (1999), but a factor of 2 uncertainty in the measured angular extent has been demonstrated by Jura (1999). We find that r_{in} may be varied between 1 and 800 AU, with the resulting 25 μm flux density contained within the *IRAS* PSC and FSC data points, and with negligible effect on the 12 μm flux density.

At 12 μm our model photosphere + cloud gives $F_{12} = 0.13$ Jy, whereas the observed *IRAS* values are 0.19 ± 0.02 Jy in the PSC and 0.25 ± 0.02 Jy in the FSC. A poor fit to the 12 μm flux was previously found in circumstellar disk models for HD 4881 (Coulson, Dent, & Dent 1998), as well as models that assume spherical dust clouds (Miroshnichenko et al. 1999). Here the 0.06 Jy difference between the flux density in our model and the PSC flux density is equal to the disagreement between the PSC and FSC flux densities. The statistical significance of the poor model fit is therefore best evaluated after follow-up 10–20 μm observations can better constrain the photometry. If the *IRAS* fluxes are confirmed, then a warm-grain component needs to be added to the model, such as from a circumstellar disk or nonequilibrium small-grain heating.

4.3. *HD 23362*

Assuming a K2 V spectral type, Sylvester et al. (1996) determined that the photometric distance to HD 23362 is 6.5 pc. This contrasts sharply against the subsequent *Hipparcos* parallax measurement that places HD 23362 at 352 pc. The derived visual extinction of ~ 2 mag (Table 3) is also inconsistent with the Sylvester et al. (1996) distance. In view of the high reddening, Sylvester et al. (1996) commented that the distance to HD 23362 should be determined independently and that the star may be misclassified.

In order to produce a closer match to the *Hipparcos* distance, we recalculate the extinction values assuming the spectral type is K2 III, with $T_{eff} = 4200$ K and $R = 20\ R_\odot$ (Tables 3 and 4). With this assumption we are then able to fit the optical and NIR photometric data with a stellar blackbody at 187 pc (Table 5; Fig. 6). The model dust cloud parameters are similar to those of HD 4881, except that there is no disagreement between the model SED and the 12 μm *IRAS* flux (Fig. 6).

Sylvester & Skinner (1996) attempted to fit the SED with a model circumstellar disk, but they failed to fit the 100 μm flux by an order of magnitude. They concluded that the 100 μm is due to infrared cirrus. Our model suggests that the 12–25 μm emission is photospheric and that all of the 60–100 μm emission is attributable to interstellar dust. Model 23362-b (Table 5, Fig. 6) indicates that R_{out} may be as small as 1.1×10^4 AU and still fit the *IRAS* PSC 100 μm data. In this case the cloud subtends $\sim 1'$ radius and would be unresolved in the IRAS 60–100 μm data.

4.4. *HD 23680*

As with HD 23362, the photometric distance for HD 23680 given the G5 V spectral type is ~ 20 pc (Sylvester & Skinner 1996), but both the *Hipparcos* parallax and the reddening are consistent with $d \sim 200$ pc. We recalculate the reddening values assuming HD 23680 has spectral type G5 III, and using $T_{eff} = 5050$ K and $R = 10\ R_\odot$, we fit the stellar SED using distance $d = 205$ pc (Table 5; Fig. 7). The cloud model (23680-a) gives satisfactory fits with $R_{out} = 7 \times 10^4$ AU, which subtends $\sim 6'$ radius. However, the second model (23680-b), with $R_{out} = 4 \times 10^4$ AU, also gives an SED passing within the error bars of the 100 μm data point. In this case, the cloud's $\sim 3'$ radius may be resolved in the 100 μm *IRAS* data. In our optical data, resolved patches of nebulosity are detected as far as 1.'7 from the star, particularly to the north-northeast, with surface brightness $R = 24$ mag arcsec^{-2}. Inspection of the ISSA at 100 μm shows an asymmetric morphology extended $\sim 3'$ north of the stellar position. Thus, the smaller outer radius for model 23680-b is preferred over model 23680-a. As with HD 23362, Sylvester & Skinner (1996) could not fit the IRAS data with a circumstellar disk model. In particular, the circumstellar disk model could not reproduce the 100 μm flux.

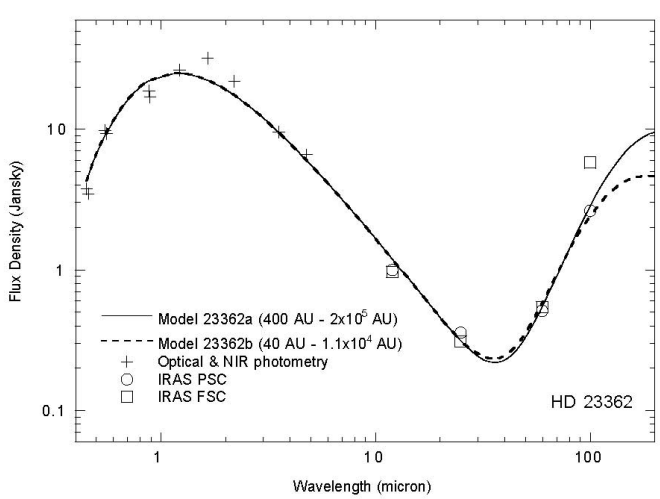

FIG. 6.—Photometric data for HD 23362 (Table 4) and spectral energy distributions from two dust cloud models (Table 5). Symbol sizes for the *IRAS* data approximate the sizes of error bars. The two models demonstrate different cloud dimensions that fit the entire 12–100 μm SED.

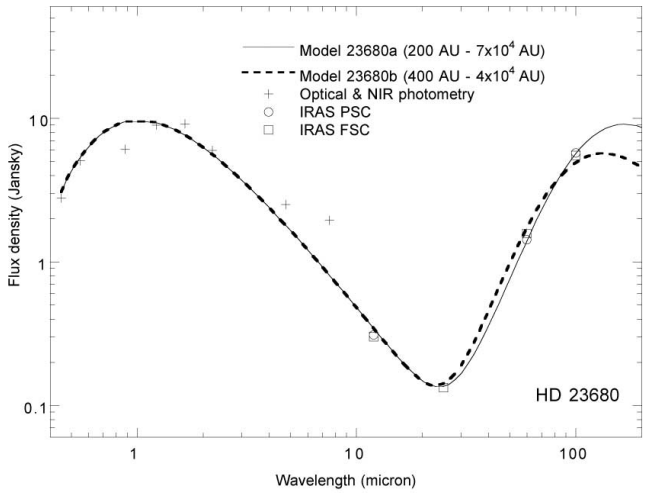

FIG. 7.—Photometric data for HD 23680 (Table 4) and spectral energy distributions from two dust cloud models (Table 5). Symbol sizes for the *IRAS* data approximate the sizes of error bars unless marked otherwise. The two models demonstrate different cloud dimensions that fit the entire 12–100 μm SED.

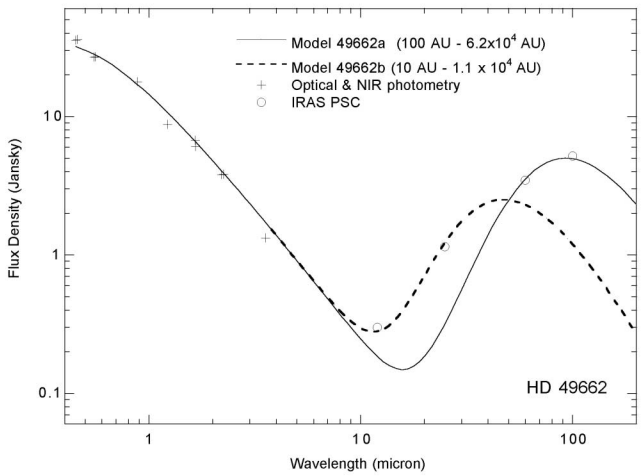

FIG. 9.—Photometric data for HD 49662 (Table 4) and spectral energy distributions from dust cloud models (Table 5). Symbol sizes for the *IRAS* data approximate the sizes of error bars. As with 18 Tau, 21 Tau, and HD 26676 (Figs. 3, 4 and 8), no single model can fit the 12–25 μm and 60–100 μm regions of the SED simultaneously. These two regions are fitted independently by models 49662-a and 49662-b (Table 5).

Rather, the simple cloud model demonstrated here is consistent with the FIR data.

4.5. *HD 26676 and HD 49662*

For both of these B stars, the dust cloud model cannot fit the 12–25 μm and 60–100 μm regions simultaneously, as was found for the Pleiads 18 Tau and 21 Tau. In Table 5 and Figures 8 and 9, we show two different models for fitting the 12–25 μm data separately from the 60–100 μm data. The models fitting the 12–25 μm emission require inner boundaries extending closer to the stars, and with greater dust number densities, than the dust cloud models that fit the 60–100 μm data. A number density distribution increasing toward the star, such as with a circumstellar disk, could also enhance the 12 and 25 μm fluxes. Thus it is possible that these stars have circumstellar disks and happen to be interacting with ISM. Alternately, the excess 12–25 μm emission could originate from nonequilibrium small-grain heating. As discussed in § 3, HD 26676 is physically associated with the Pleiades. Castelaz et al. (1987) demonstrated that nonequilibrium grain heating in the Pleiades nebulosity produces $\sim$30% of the total 12–100 μm emission at 12 and 25 μm. Models 26676-a and 49662-a in Figures 8 and 9 generate only $\sim$10% of the total observed emission at 12–25 μm. Thus, an added small-grain component could alter the resulting SED to fit the data. If this is true, then evidence should also exist for NIR excess or infrared emission features (Sellgren et al. 1996). We have no NIR data for HD 26676, but the NIR data for HD 49662 is consistent with a purely photospheric origin. The scale of emission for models HD 26676-a and HD 49662-a, given the distances listed in Table 5, is $\sim$5.′5, which is consistent with the $\sim$10′ radii measured by Gaustad & Van Buren (1993) in *IRAS* Skyflux plates.

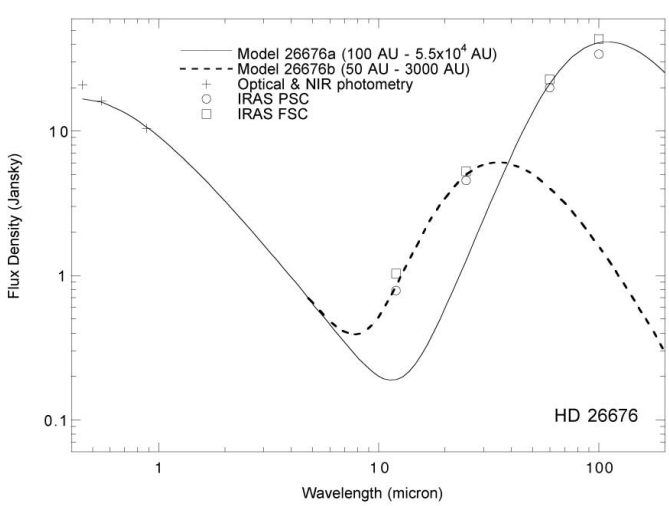

FIG. 8.—Photometric data for HD 26676 (Table 4) and spectral energy distributions from two dust cloud models (Table 5). Symbol sizes for the *IRAS* data approximate the sizes of error bars. As with the Pleiads 18 Tau and 21 Tau (Figs. 3 and 4), no single model can fit the 12–25 μm and 60–100 μm regions of the SED simultaneously. These two regions are fitted independently by models 26676-a and 26676-b.

4.6. *HD 123160*

The photometric distance of 16 pc assuming that HD 123160 is a G5 V star (Sylvester et al. 1996) is inconsistent with the lack of parallax information from the *Hipparcos* and Gliese catalogs and with the high extinction (Table 3). Although we confirm that the optical and NIR data may be fitted with a G5 V star at 16 pc, a nearly equal model SED is obtained by assuming a G0 III star at $\sim$110 pc. For either spectral type the visual extinction exceeds 2 mag (Table 3). In Figure 10 and Table 5 we present dust cloud models assuming HD 123160 is a distant giant. However, further study of this system is necessary to determine its evolutionary status. Lithium abundance measurements suggest that HD 123160 is relatively young, with an age of $\sim$70 Myr (Dunkin, Barlow, & Ryan 1997). This age is comparable to that of many Vega-like stars as well as members of the Pleiades. The nebulosities iia and iib (Fig. 2) may originate from the same physical mechanisms that produce the IC 349 nebulosity near 23 Tau in the Pleiades (Herbig 1996;

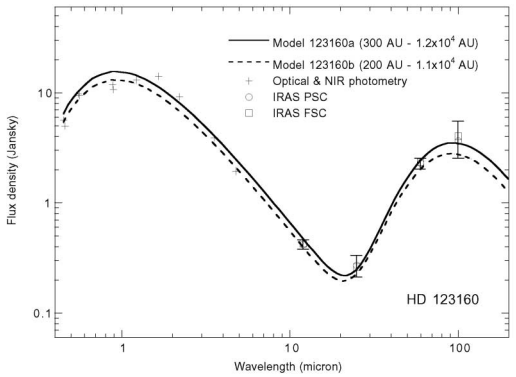

FIG. 10.—Photometric data for HD 123160 (Table 4) and spectral energy distributions from dust cloud models (Table 5). Symbol sizes for the *IRAS* data approximate the sizes of error bars unless marked otherwise. The two models demonstrate different cloud radii that fit the data. With model 123160-b, we demonstrate that the distance could be increased to $d = 120$ pc and still obtain a satisfactory fit to the SED between 0.45 and 12 μm.

Herbig & Simon 2001). The semistellar appearance of iia is similar to the main knot in IC 349 (Herbig 1996; Herbig & Simon 2001), except that it is very red (§ 3). On the other hand, the entire complex of nebulous features shown in Figure 1*F* resembles a star-forming region where a young star illuminates its natal dust cloud. Feature iia could be a K star associated with HD 123160. The SEDs produced by our Pleiades cloud model fit the observed 12–100 μm data points (Fig. 10), and the scale of emission for the models is $\sim$1.″5 radius. This corresponds to the projected separation between HD 123160 and feature iv (Fig. 4*f*). A circumstellar disk model used by Sylvester & Skinner (1996), assuming HD 123160 is a G5 V star at 16 pc, also gives satisfactory fits to the data. However, the present high-resolution data (Fig. 2) show no evidence for a circumstellar disk, and we therefore favor the Pleiades cloud model.

5. DISCUSSION

Backman & Paresce (1993) cautioned that thermal emission from reflection nebulosities such as in the Pleiades may appear similar to thermal emission from Vega-like stars. Our simulations of interstellar grain emission demonstrate that the nebulae shown in Figure 1 are capable of producing the excess thermal emission observed by *IRAS*. In three cases, a circumstellar disk or nonequilibrium small-grain heating may account for the 12–25 μm emission. The latter mechanism is consistent with our current understanding of grain emission from the Pleiades.

A general problem in interpreting SEDs is that the models typically have as many adjustable parameters as there are data points. Good fits are not persuasive by themselves to determine the distribution of the dust, especially when the dust is optically thin to absorption and emission. Unlike the SEDs of young stellar objects, the Vega-like stars have strongly peaked FIR flux densities consistent with dust with a small range of temperatures. To interpret the dust distributions as lying in a single plane (disks) requires additional information, such as images of the scattered light.

Other authors have fitted the *IRAS* data for HD 4881, HD 23362, HD 23680, and HD 123160 with circumstellar disk models and in some cases interpreted excess emission at 100 μm as due to infrared cirrus (Low et al. 1984) in the background. Given the optical data and the results of our modeling, we argue that the infrared cirrus is local to each star, appearing as the Pleiades phenomenon in scattered light. From the infrared standpoint, the term "cirrus hot spot" is used to describe the local heating of ISM by a star. To qualify as cirrus hot spots, FIR emission must be extended on arcminute scales with color temperatures between 25 and 70 K (Gaustad & Van Buren 1993). The early-type stars in the Pleiades, for example, appear as cirrus hot spots in the *IRAS* data. The three B stars in our list, HD 4881, HD 26676, and HD 49662, are also identified as infrared cirrus hot spots (Gaustad & Van Buren 1993; Dring et al. 1996).

Our three B stars, as well as 18 Tau and 21 Tau from the original sample, are given as Vega excess stars by Backman & Paresce (1993) in their Table VIII. We find that all but three of the remaining 29 B stars in the Backman & Paresce (1993) table are also identified as cirrus hot spots by Gaustad & Van Buren (1993). The two different interpretations for the same FIR data illustrate the difficulty in uniquely identifying the origin of dust that produces excess thermal emission. For instance, Backman & Paresce (1993) identified Vega-like stars if the color temperature satisfied $30\ \mathrm{K} < T < 500\ \mathrm{K}$, which overlaps the color temperature criterion adopted by Gaustad & Van Buren (1993). However, the Vega-like stars with resolved debris disks and rings (e.g., β Pic, ϵ Eri, Fomalhaut, HR 4796A) have heliocentric distances $d < 100$ pc, whereas the stars discussed here are located at $d > 100$ pc. Thus the unique identification of thermal excess is problematic for the more distant objects. From our initial sample of 79 Vega-like stars, 72 have *Hipparcos*-detected distances, and of these 43 (60%) have $d > 100$ pc. In part, the source confusion is a question of spatial resolution. Resolved observations from the optical to the far-infrared are essential for determining the nature of circumstellar dust. However, the Sun also lies within a relatively ISM-free bubble 65–250 pc in radius (Sfeir et al. 1999). Thus, the Pleiades phenomenon naturally occurs with greater frequency among the more distant stars.

Although distance is a first-order measure for the reliability of identifying the Vega phenomenon, the Local Bubble has a nonspherical geometry, giving specific directions with respect to the Sun that are most likely to contain denser ISM that would produce the Pleiades phenomenon. Sfeir et al. (1999) use the Na I D-line doublet to measure absorption toward stars within 300 pc of the Sun and produce maps of neutral gas in three Galactic projections. In Figures 11, 12, and 13, we plot the locations of Vega-like stars using the same Galactic projections as Sfeir et al. (1999). We take the 60 Vega-like stars from Backman & Paresce's (1993) Table VIII ("Bright star catalog main-sequence stars with Vega-like far-infrared excesses") and 73 Vega-like stars from Mannings & Barlow's (1998) Table 2 ("Newly identified candidate main-sequence stars with debris disks"). Two stars (HD 73390 and HD 181296) in Mannings & Barlow (1998) are in the Backman & Paresce (1993) table, leaving a total sample of 131 stars. From this sample we select the 111 stars that have *Hipparcos*-detected distances. Finally, a total of 85 Vega-like stars lie within the three planes of reference defined by Sfeir et al. (1999), and those within 300 pc of the Sun are plotted in Figures 11–13. We overlay two contours that trace the lowest and highest Na I D2 absorption mapped by Sfeir et al. (1999). The figure captions give more details.

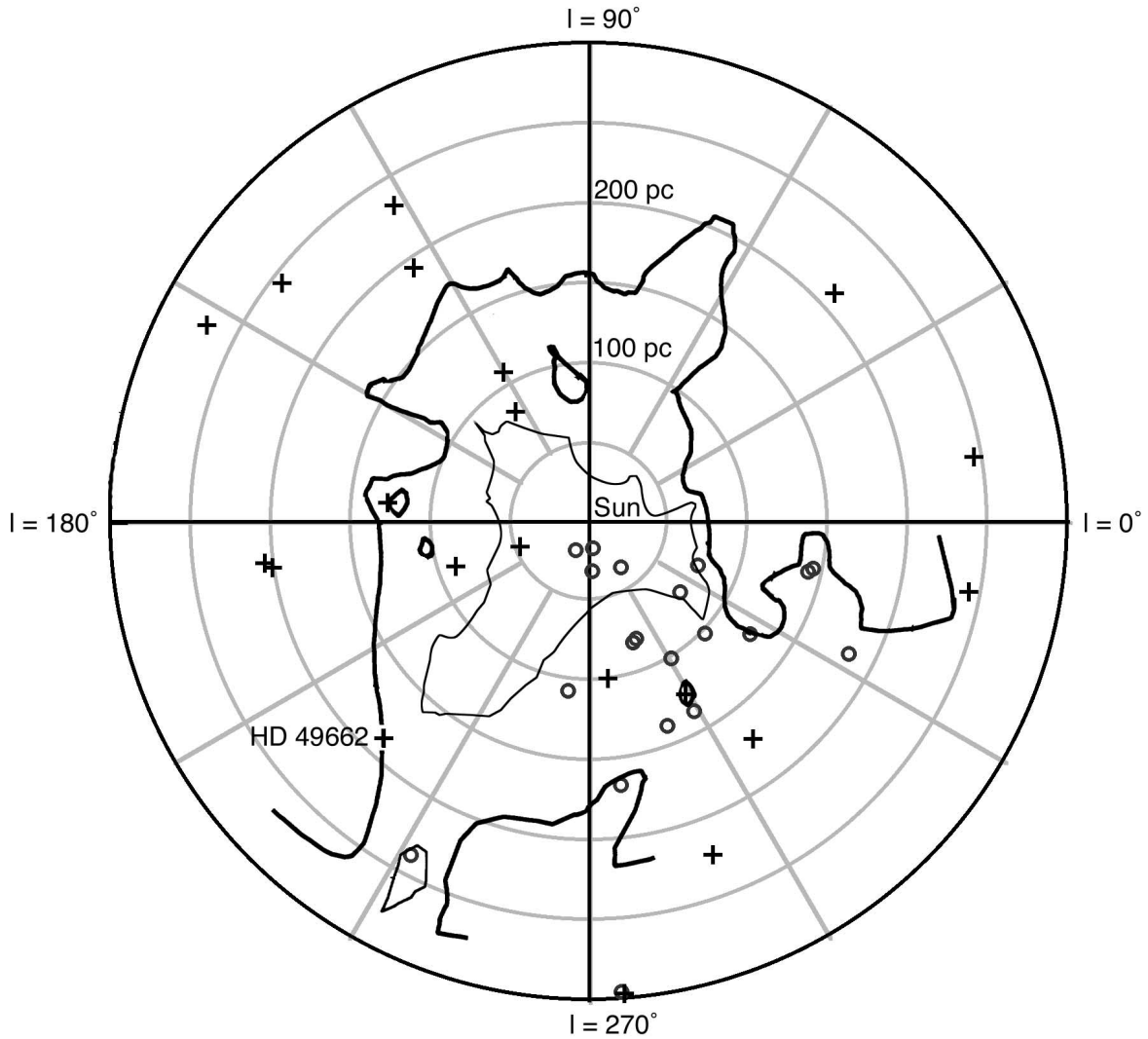

FIG. 11.—Galactic plane (*downward*) view of Vega-like stars from Backman & Paresce 1993 (*crosses*) and Mannings & Barlow 1998 (*circles*). The Sun is at the center. Following Sfeir et al. (1999), only stars that have $-18° < b < 18°$ are plotted, and the Sun–star distance is the *Hipparcos* distance irrespective of the angle above or below the reference plane. The isocontours trace the Na I gas absorption from Fig. 3 in Sfeir et al. (1999). The thin and thick contours correspond to the 5 mÅ and >50 mÅ D2-line equivalent widths, respectively. One exception is the closed contour near $l = 240°$, $d = 250$ pc which traces a 20 mÅ equivalent width isocontour from Sfeir et al. (1999). We show it because the Vega-like source HD 52140 falls within the contour boundary. Two more examples of Vega-like stars associated with local overdensities of gas are HD 28149 at $l = 174°$, $d = 127$ pc and HD 108257 at $l = 299°$, $d = 123$ pc.

Figures 11–13 show that the walls of the Local Bubble approach the Sun to less than 50 pc in certain directions but are more than 100 pc distant in other directions, particularly toward the North Galactic Pole (Fig. 13; named the "Local Chimney" by Welsh et al. 1999). In the Galactic plane view (Fig. 11) the Local Bubble has maximum extent toward $l = 225°$, which is also the direction toward HD 49662. However, HD 49662 is located right on the wall of the high-density gas. Three more Vega-like stars in Figure 11 (HD 52140, HD 28149, and HD 108257) appear spatially associated with local overdensities of gas.

Figure 12 shows that HD 23680 is in the same general direction of HD 26676 and both are within the region of high-density gas. Also evident is a group of five stars that trace the high-density wall at $l = 180°$, $b \sim -30°$, $d \sim 125$ pc. These Vega-like stars (HD 23324 = 18 Tau, HD 23432 = 21 Tau, HD 28149, HD 28375, and HD 28978) are associated with Taurus and the Pleiades. Two more groups of five stars each appear in Fig. 12. At $l = 0°$, $b \sim -30°$, $d \sim 50$ pc we find HD 181296, HD 191089, HD 176638, HD 181864, and HD 181327. These are not associated with gas, but HD 181296 and HD 181327 are members of the Tucanae Association (Zuckerman & Webb 2000). Their youth and the lack of interstellar gas favors the Vega phenomenon interpretation of their FIR excesses. A third group of Vega-like stars is evident at $l = 0°$, $b \sim 25°$, 100 pc $< d <$ 150 pc (HD 142096, HD 142165, HD 143018, HD 145263, and HD 145482). These are at the distance and direction of the Upper Scorpius subgroup of the Sco OB2 association (de Zeeuw et al. 1999), which is encompassed by a giant reflection nebula (Gordon et al. 1994). The association of these stars with large-scale dust and gas favors the Pleiades phenomenon interpretation for the FIR excesses.

Figure 13 shows that Vega-like stars may be detected at the greatest distances with the least confusion from the ISM in the direction of the North Galactic Pole. The figure also shows a group of four stars at $l = 90°$, $b \sim -30°$, $d \sim 20$ pc (HD 39060 = β Pic, HD 41742, HD 53143, and HD 67199).

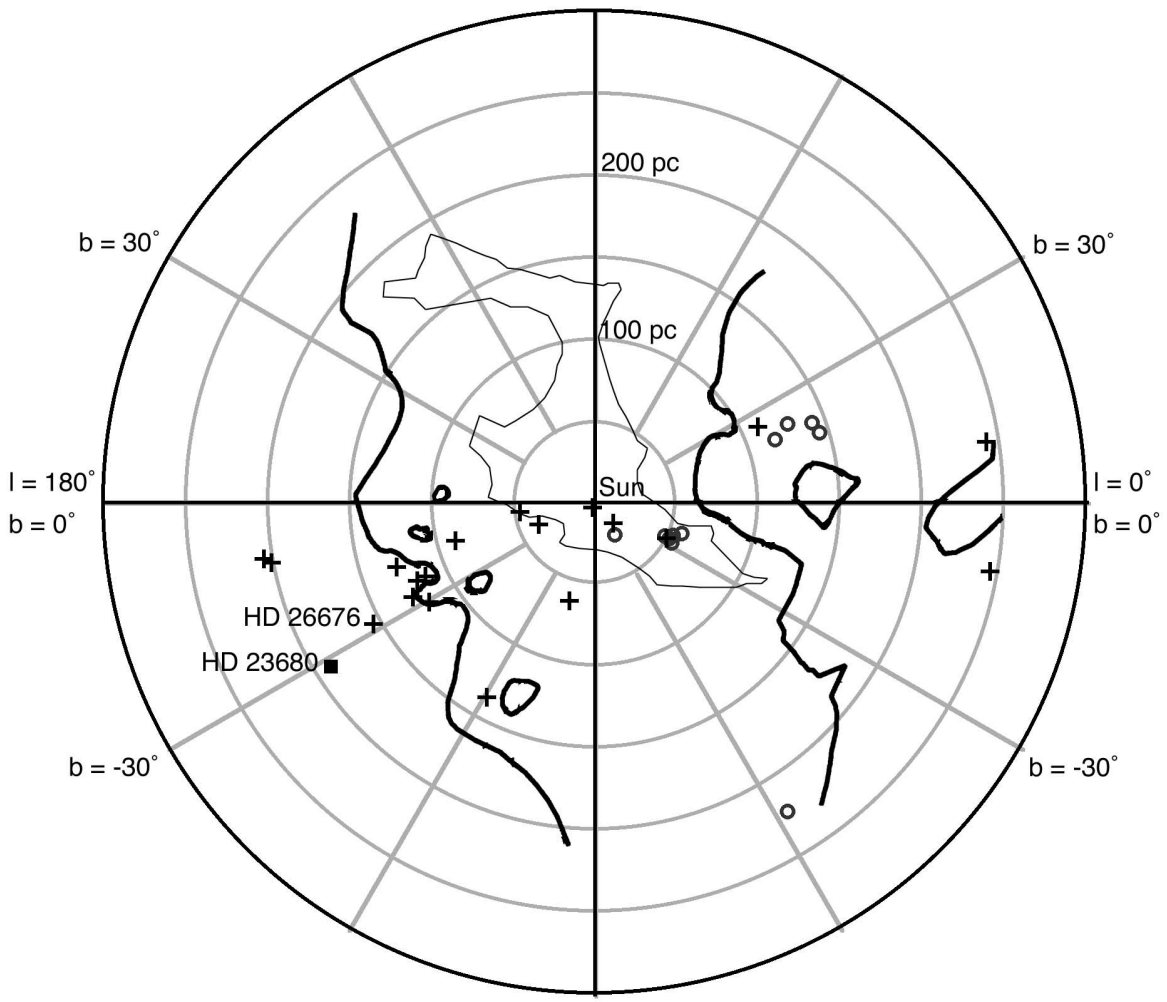

FIG. 12.—Meridian plane view, perpendicular to the Galactic plane, and containing both Galactic poles and the Galactic center to the right. Symbols and contours same as Fig. 11. Stars are plotted if they fall within $l = 0° \pm 18°$ or $l = 180° \pm 18°$. HD 23680 from our study falls within these limits and is plotted with a solid square.

Their location in the Local Bubble and their association with β Pic favors the Vega phenomenon explanation for their FIR excesses.

Overall, the fraction of Vega-like stars that lie at or beyond the Local Bubble wall (*thin contour*) is greater than 50%. In Figure 11 we plot 40 Vega-like stars, but only five are in the Local Bubble. The remainder are located at or beyond the wall of low-density gas, and 16 of these are in high-density gas regions. Another 11 stars from the Backman & Paresce (1993) and Mannings & Barlow (1998) tables would appear in Figure 11 if we plotted distances between 300 and 600 pc. From the 30 Vega-like stars plotted in Figure 12, 16 are in the high-density gas and six more lie between the high-density and low-density walls. In Figure 13, six Vega-like stars are in the Local Bubble, four lie between the low- and high-density walls, and four more are found in the high-density regions.

Not only are the post-*Hipparcos* distance determinations useful for judging the position of Vega-like stars relative to the Local Bubble, they also help evaluate the physical scale of thermal emission. We found that the *Hipparcos* parallaxes for HD 23362, HD 23680, and HD 123160, as well as the large reddening values, probably place these stars beyond 100 pc, rather than at 6–16 pc, as determined in pre-*Hipparcos* investigations. The greater distances therefore explain how the thermal emission may originate from ISM material extending 10^3–10^5 AU from each star and still meet the criteria for inclusion in the *IRAS* PSC. The possibility that these stars are distant giants producing the Pleiades phenomenon may help explain the infrared excesses observed around $\sim$100 luminosity class III stars (Zuckerman, Kim, & Liu 1995; Jura 1999; Kim, Zuckerman, & Silverstone 2001).

6. SUMMARY

We detect optical reflection nebulosity around six main-sequence stars that are candidates for having debris disks. Five nebulae share the morphological characteristics of dust surrounding bright stars in the Pleiades. The environment of HD 123160 has features that resemble both the Pleiades and star-forming regions. No disklike structures are detected, although our optical coronagraphic technique does not probe the circumstellar environment closer than $\sim$4″ radius. The sensitivity-limited radii of the nebulosities

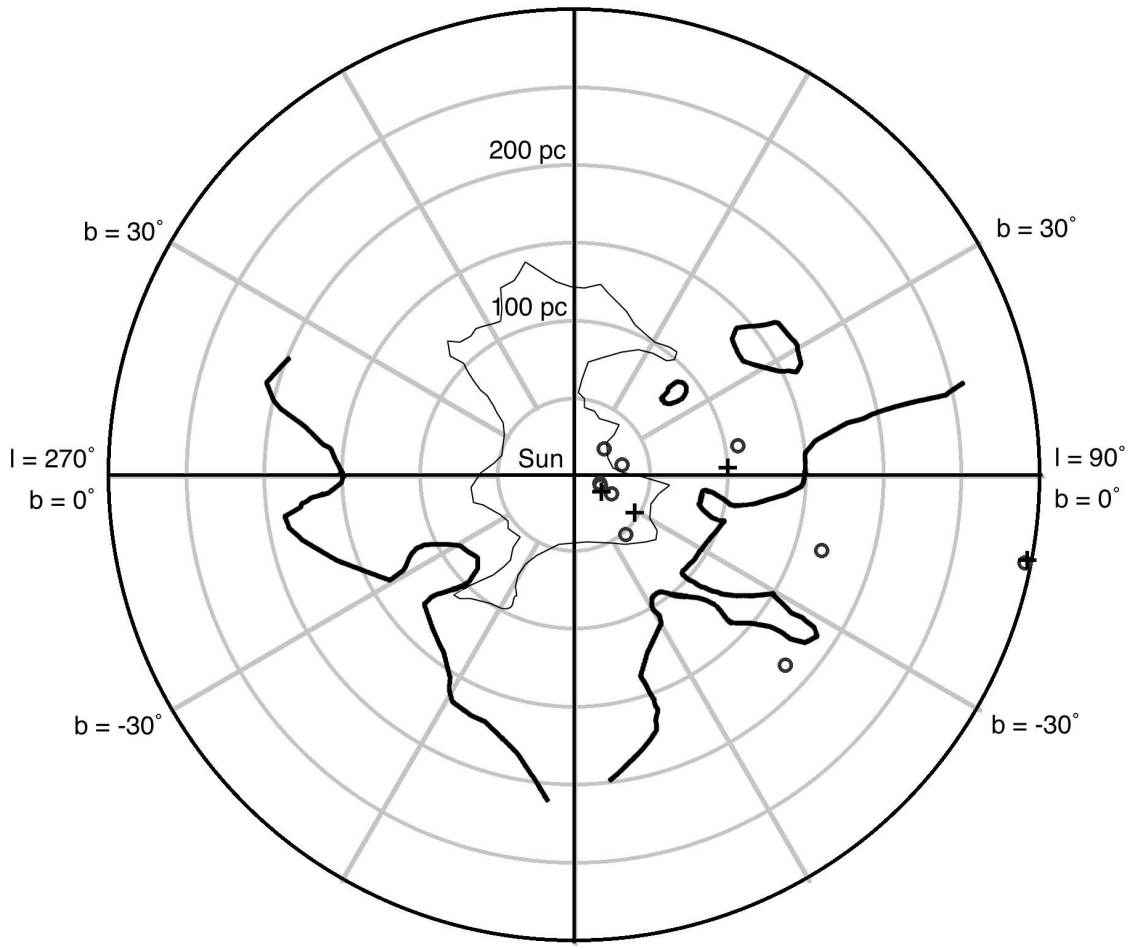

FIG. 13.—Galactic rotation plane, perpendicular to both the Galactic plane and to the Galactic center direction. Symbols and contours same as Fig. 11. Stars are plotted if they fall within $l = 90° \pm 18°$ or $l = 270° \pm 18°$.

are between 1′ and 2′, and the radial measurements of surface brightness are consistent with uniform density dust clouds illuminated by the central star.

We show that thermal emission from an optically thin, uniform density dust cloud surrounding HD 23362, HD 23680, and HD 123160 can entirely explain the 12–100 μm emission detected by *IRAS*. The Pleiades phenomenon, a random encounter between a clump of ISM and a star, is the most likely explanation for the excess FIR emission. For HD 4881, HD 26676, and HD 49662, the blackbody cloud model cannot simultaneously fit the 12–25 μm and 60–100 μm regions of the *IRAS*-detected SED. These stars may have circumstellar disks in addition to the interstellar dust detected in the optical. However, the excess 12–25 μm emission may also arise from nonequilibrium heating of small grains. We show that 18 Tau and 21 Tau in the Pleiades have comparable SEDs with signatures of hot grains in the 12–25 μm fluxes. Future observations sensitive to disklike structure within 500 AU of each star and that search for NIR excesses and emission features are necessary to determine if these stars are manifesting the Vega phenomenon and the Pleiades phenomenon simultaneously.

We find that most Vega-like B stars have also been associated with FIR cirrus hot spots. We demonstrate that more than 50% of Vega phenomenon stars are located beyond the gas-poor Local Bubble, and many are spatially associated with regions of high-density neutral gas. Thus, a significant fraction of Vega phenomenon stars beyond 100 pc may be confused with Pleiades phenomenon stars.

We are grateful to J. Gradie, B. Zuckerman, and E. Becklin for access to their coronagraph. This work was supported in part by NASA grants to D. C. J. and P. K. and by the NSF Center for Adaptive Optics, managed by University of California, Santa Cruz, under cooperative agreement AST 98-76783. This research has made use of the NASA/IPAC Infrared Science Archive, which is operated by the Jet Propulsion Laboratory, California Institute of Technology, under contract with NASA.

REFERENCES

Arny, T. 1977, ApJ, 217, 83
Artymowicz, P., & Clampin, M. 1997, ApJ, 490, 863
Aumann, H. H. 1988, AJ, 96, 1415
Aumann, H. H., et al. 1984, ApJ, 278, L23
Backman, D. E., & Gillett, F. C. 1987, in Cool Stars, Stellar Systems, and the Sun, ed. J. L. Linsky & R. E. Stencel (Berlin: Springer), 340
Backman, D. E., & Paresce, F. 1993, in Protostars and Planets III, ed. E. H. Levy & J. I. Lunine (Tucson: Univ. Arizona Press), 1253
Castelaz, M. W., Sellgren, K., & Werner, M. W. 1987, ApJ, 313, 853
Coulson, I. M., Dent, D. M., & Dent, W. R. F. 1998, MNRAS, 296, 934
Cox, A. 1999, Allen's Astrophysical Quantities (New York: AIP)
Desert, F.-X., Boulanger, F., & Puget, J. L. 1990, A&A, 237, 215
de Zeeuw, P. T., Hoogerwerf, R., de Bruijne, J. H. J., Brown, A. G. A., & Blaauw, A. 1999, AJ, 117, 354
Dring, A. R., Murthy, J., Henry, R. C., & Walker, H. J. 1996, ApJ, 457, 764
Dunkin, S. K., Barlow, M. J., & Ryan, S. G. 1997, MNRAS, 290, 165
Gaustad, J. E., & Van Buren, D. 1993, PASP, 105, 1127
Gordon, K. D., Witt, A. N., Carruthers, G. R., Christensen, S. A., & Dohne, B. C. 1994, ApJ, 432, 641
Greenberg, J. M. 1968, in Nebulae and Interstellar Matter, ed. B. M. Middlehurst & L. H. Aller (Chicago: Univ. Chicago Press), 221
Herbig, G. H. 1996, AJ, 111, 1241
Herbig, G. H., & Simon, T. 2001, AJ, 121, 3138
Jura, M. 1999, ApJ, 515, 706
Kalas, P. 1998, Earth, Moon, Planets, 81, 27
Kim, S. S., Zuckerman, B., & Silverstone, M. 2001, ApJ, 550, 1000
Lagrange, A.-M., Backman, D. E., & Arymowicz, P. 2000, in Protostars and Planets IV, ed. V. Mannings, A. P. Boss, & S. S. Russell (Tucson: Univ. Arizona Press), 1253
Lloyd, J. P., Liu, M. C., Macintosh, B. A., Severson, S. A., Deich, W. T. S., & Graham, J. R. 2000, Proc. SPIE, 4008, 814
Low, F. J., et al. 1984, ApJ, 278, L19
Mannings, V., & Barlow, M. J. 1998, ApJ, 497, 330
Mathis, J. S. 1990, ARA&A, 28, 37
Max, C. E., et al. 1997, Science, 277, 1649
Meyer, M. R., Calvet, N., & Hillenbrand, L. A. 1997, AJ, 114, 288
Miroshnichenko, A. S., Mulliss, C. L., Bjorkman, K. S., Morrison, N. D., Kuratov, K. S., & Wisniewski, J. P. 1999, MNRAS, 302, 612
Nakajima, T., & Golimowski, D. A. 1995, AJ, 109, 1181
Plets, P. 1999, A&A, 343, 496
Racine, R. 1968, AJ, 73, 233
Sellgren, K. 1984, ApJ, 277, 623
Sellgren, K., Luan, L., & Werner, M. W. 1990, ApJ, 359, 384
Sellgren, K., Werner, M. W., & Allamandola, L. J. 1996, ApJS, 102, 369
Sfeir, D. M., Lallement, R., Crifo, F., & Welsh, B. Y. 1999, A&A, 346, 785
Sylvester, R. J., & Skinner, C. J. 1996, MNRAS, 283, 457
Sylvester, R. J., Skinner, C. J., & Barlow, M. J. 1997, MNRAS, 289, 831
Sylvester, R. J., Skinner, C. J., Barlow, M. J., & Mannings, V. 1996, MNRAS, 279, 915
van den Bergh, S. 1966, AJ, 71, 990
Welsh, B. Y., Sfeir, D. M., Sirk, M. M., & Lallement, R. 1999, A&A, 352, 308
White, R. E., & Bally, J. 1993, ApJ, 409, 234
Zuckerman, B., Kim, S. S., & Liu, T. 1995, ApJ, 446, L79
Zuckerman, B., & Webb, R. A. 2000, ApJ, 535, 959